Title
Complex conductivity response to silver nanoparticles in partially saturated sand columns

Authors
Aal, Gamal Abdel
Atekwana, Estella A
Werkema, D Dale

Publication Date
2017-02-01

DOI
10.1016/j.jappgeo.2016.12.013

Peer reviewed

Published in final edited form as:
J Appl Geophy. 2017 February ; 137: 73–81. doi:10.1016/j.jappgeo.2016.12.013.

Complex conductivity response to silver nanoparticles in partially saturated sand columns

Gamal Abdel Aal[a,b], **Estella A. Atekwana**[a,*], **D. Dale Werkema Jr**[c]

[a]Oklahoma State University, Stillwater, OK, USA

[b]Geology Department, Faculty of Science, Assuit University, Assiut, Egypt

[c]U.S. Environmental Protection Agency, ORD, NERL, EMMD, ECB, Las Vegas, NV, USA

Abstract

The increase in the use of nanoscale materials in consumer products has resulted in a growing concern of their potential hazard to ecosystems and public health from their accidental or intentional introduction to the environment. Key environmental, health, and safety research needs include knowledge and methods for their detection, characterization, fate, and transport. Specifically, techniques available for the direct detection and quantification of their fate and transport in the environment are limited. Their small size, high surface area to volume ratio, interfacial, and electrical properties make metallic nanoparticles, such as silver nanoparticles, good targets for detection using electrical geophysical techniques. Here we measured the complex conductivity response to silver nanoparticles in sand columns under varying moisture conditions (0–30%), nanoparticle concentrations (0–10 mg/g), lithology (presence of clay), pore water salinity (0.0275 and 0.1000 S/m), and particle size (35, 90–210 and 1500–2500 nm). Based on the Cole-Cole relaxation models we obtained the chargeability and the time constant. We demonstrate that complex conductivity can detect silver nanoparticles in porous media with the response enhanced by higher concentrations of silver nanoparticles, moisture content, ionic strength, clay content and particle diameter. Quantification of the volumetric silver nanoparticles content in the porous media can also be obtained from complex conductivity parameters based on the strong power law relationships.

Keywords

Nanoparticles; Complex conductivity; Nanosilver; Environmental nanomaterials

1. Introduction

The unique physicochemical properties of nanoparticles such as their small size, reactivity, morphology and surface chemistry has resulted in their rapid adaptation and use in consumer goods, technical, manufacturing, medicine, industrial, and remediation technologies (e.g., Delay and Frimmel, 2012; Shi et al., 2015). The Woodrow Wilson International Center

*Corresponding author at: Boone Pickens School of Geology, Oklahoma State University, 105 Noble Research Center, Stillwater, OK 74078, USA. estella.atekwana@okstate.edu (E.A. Atekwana).

for Scholars and the Project on Emerging Nanotechnologies recent update of the Nanotechnology Consumer Products Inventory includes over 1800 consumer products (Vance et al., 2015). Such rapid growth in the application of nanomaterials (NMs) spawned the new field of nanotoxicology to determine the safety of engineered nanomaterials (ENMs), engineered nanoparticles (ENPs), as well as developing advanced laboratory characterization methods (Hussain et al., 2015). Due to the potential cellular modifications of ENMs, nanotoxicology has grown to focus on understanding the mechanisms behind cellular alterations to biological systems (Hussain et al., 2015). The general consensus is that the increasing use of nano-scale materials in commercial products will also increase the likelihood, and some say inevitability (Cuny et al., 2015) of human and ecological exposures to these materials either through intentional introduction via remediation activities (Busch et al., 2015; Braunschweig et al., 2013; Rakshit et al., 2013; Tosco et al., 2014; Shi et al., 2015) or accidental introduction to the environment through landfill leaks, or wastewater treatment discharge into the environment (Handy et al., 2008; Bouchard et al., 2009; Benn et al., 2010; Thakkar et al., 2010; Gerloff et al., 2012; Gottschalk et al., 2013; Luque-Garcia et al., 2013). Once in the environment, the fate and transport of ENPs within subsurface environs and surface water systems is largely unknown (Cornelis et al., 2013). This is disconcerting as there is some evidence for the toxic effects of ENPs on organisms as well as damage to the cell membranes (e.g., Asharani et al., 2008; Navarro et al., 2008; Hussain et al., 2015). Within the subsurface, the transport characteristics and retention in porous media are determined by their interaction with the solid components of the subsurface (Cuny et al., 2015). Cuny et al. (2015) provide a good overview for interested readers, of the three main mechanisms for the fate and transport of ENMs; interception, gravitational sedimentation, and Brownian diffusion. These mechanisms have lead many researchers to use breakthrough curves (BTCs) to investigate the behavior of ENMs within porous media (e.g. Hosseini and Tosco, 2013; Cornelis et al., 2014; Cuny et al., 2015). Recent research on the fate and transport of nanoparticles highlight the concern of their presence in the environment (Cornelis et al., 2014; Cuny et al., 2015) and show NPs transport in the subsurface may not be hydrologically intuitive as gravity driven flow was found to decrease the transport of metal-oxide NPs in porous media (Cai et al., 2015); thus, supporting the need for continued NP transport studies.

Of the many consumer products, nanosilver (AgNPs) is reported to occur within 24% of the products that list the type of nanomaterial used; thus, classifying AgNPs as the most used within these products (Vance et al., 2015). Due to its antimicrobial properties, AgNPs products contain silver ranging from 0.0014 mg to 270 mg Ag per gram of product (Benn et al., 2010). Within the natural environment, the low redox potential of AgNPs may increase its possible release into the subsurface (Ivanova and Zamborini, 2009). Among metal nanoparticles, silver nanoparticles (AgNPs) possess many superior properties attractive for consumer products, such as increased electrical conductivity, antimicrobial activity, and catalytic effect, for example (Kabashin et al., 2003). Hence, AgNPs are by far the most widely used engineered NPs (Boxall et al., 2007; Kim et al., 2007; Blaser et al., 2008; Klaine et al., 2008; Ma et al., 2010; Vance et al., 2015) and; therefore, the NP of choice for this study.

Unfortunately, due to their nanoscale size, high reactivity, and ill-defined dissolution properties, AgNPs environmental risks are considered very difficult to determine (Benoit et al., 2013). In addition, identifying the potential risks of AgNPs associated with their nanoscale structure has been difficult due to the fundamental challenge of detecting and monitoring nanoparticles in the environment (Glover et al., 2011). Despite our knowledge of likely AgNPs environmental release pathways, information on AgNPs in the soil system is lacking as their environmental fate and transport may depend on their mobility in the vadose zone. Thus, the vadose zone likely provides a sink for nanomaterials due to solid particle deposition and pore straining, preventing their spread, or a long-term contaminant source (Chen and Elimelech, 2008; Cuny et al., 2015). Most ENM studies were performed under saturated conditions; but unsaturated or partially saturated conditions occurring within the vadose zone represent the potential pathway for ENMs introduction to the subsurface after surface accidental spills or releases. For example, Prédélus et al. (2015) investigated the mobility of nanoparticles and a bromide tracer through the vadose zone using a lysimeter. Their findings show that 80% of the nanoparticles were retained within the lysimeter showing the effect of a capillary barrier on nanoparticle transport and highlighting the importance of understanding unsaturated flow for subsurface nanoparticle fate and transport (Prédélus et al., 2015). The accumulated environmental concentrations of nanoparticles also remain unknown as analytical methods that are specific for ENP detection and quantification are improving (Hussain et al., 2015), but are generally limited due to their small size and challenging morphology (Gottschalk et al., 2013). Important environmental, health, and safety research needs for ENPs include: quantitative knowledge and methods for their detection, characterization and quantification, as well as understanding their fate and transport in complex natural media (e.g., Gottschalk et al., 2013). Therefore, demand exists for the development of techniques to detect and quantify their presence in the subsurface using in-situ detection methods.

Compared with conventional soil and water sampling and laboratory analysis, near surface geophysical techniques provide such a potential by measuring in-situ conditions without direct sampling. In contrast, chemical, electrochemical, microscopic, and spectroscopic analyses require a sample to be extracted from in-situ conditions (i.e., creating an environmentally disturbed sample) and measured in the laboratory Shi et al. (2015) provide a thorough overview of such laboratory analysis and for the use of complex conductivity for nZVI detection. To our knowledge, only Joyce et al. (2012) and Shi et al. (2015) utilize a geophysical method, complex conductivity, for the detection and characterization of ENMs within saturated laboratory column experiments. Among geophysical methods, choosing complex conductivity is intuitive, due to the small size of ENPs, high surface area to volume ratio, and Ag electrical conductivity which all make metallic ENPs ideal targets for detection with low frequency electrical geophysical techniques (Joyce et al., 2012). Although the geophysical measurement is indirect and typically requires petrophysical models to estimate physicochemical characteristics, complex conductivity (also referred to as spectral induced polarization (SIP)) is a well-established geophysical method that has been shown to be sensitive to the presence of disseminated metals and very small physiochemical changes occurring at the grain fluid interface (e.g. Seigel et al., 1997; Slater et al., 2005, 2006; Wu et al., 2005; Mansoor and Slater, 2007; Gurin et al., 2013). In fact, a number of investigations

have demonstrated the utility of detecting microbially-induced nano-scale metal precipitates (Ntarlagiannis et al., 2005; Williams et al., 2005, 2009) using this technique.

1.1. Electrical theory

Complex conductivity, or Spectral induced polarization (SIP), measures the ability of porous materials to store reversible electrical charges or capacitance (see a thorough review of the method in Revil et al., 2012). This polarization is due to the application of an external current source and is characteristic of a material's ability to store a charge. In practice, current is injected into the subsurface or a volume of sample (for laboratory measurements) across a wide range of frequencies (typically from 1 mHz to few tens of kHz (< 100 Hz in field conditions)). The complex conductivity is measured as a conductivity magnitude $|\sigma|$ and the phase shift ϕ of the measured signal relative to the transmitted current. As a result, the in-phase (real conductivity) and quadrature (imaginary or out-of phase) conductivities can be calculated from the measured magnitude $|\sigma|$ and phase shift ϕ of the sample as follows:

$$\sigma' = |\sigma| \cos\phi, \tag{1}$$

$$\sigma'' = |\sigma| \sin\phi. \tag{2}$$

Where the in-phase (σ') conductivity component represents ohmic conduction and is sensitive to fluid chemistry, and contains an electrolytic and interfacial component (Waxman and Smits, 1968; Lesmes and Frye, 2001). The surface conductivity occurs via the formation of an electrical double layer (EDL) at the grain-fluid interface (Revil and Glover, 1998; Schmutz et al., 2010). The out of phase (quadrature or imaginary) conductivity σ'' represents the polarization term associated with the reversible storage of electrical charges in porous media and is sensitive to physicochemical properties at the fluid-grain interface (e.g., surface area, surface charge density, ionic mobility, and tortuosity). At low frequencies (< 1 kHz), several conduction and polarization mechanisms can exist in metal containing sediments (Wu et al., 2005; Slater et al., 2006; Wu et al., 2009). A complex interfacial conductivity represents the conduction and polarization processes occurring at the metal/electrolyte interface, whereas an electronic conduction term accounts for conduction via interconnected electronically conductive metals. The complex conductivity of the metallic particles incorporates both conduction and polarization within the electrical double layer (EDL) occurring at the electrolyte/metal mineral interface, which includes a diffusive mechanism associated with ion migration to and from the metallic surface (Wong, 1979; Slater et al., 2005) as well as an electrochemical mechanism associated with redox active ions that transfer electrons across the mineral/electrolyte interface. This transfer occurs via redox reactions, to the particle that can be an electronic conductor or a semi-conductor (Wong, 1979). Whereas the measured in-phase conduction component depends on electrolytic conduction, electronic conduction, and interfacial conduction; the quadrature conductivity is only dependent on the interfacial properties of metals (or subsurface solid particles). Deconvolving these conduction mechanisms yield material physicochemical

characteristics important for understanding the complex conductivity response to samples containing AgNPs.

In the current study, we provide a first attempt to investigate the sensitivity of the complex conductivity technique to the presence of AgNPs under partially saturated conditions using concentrations likely to be found in the environment. Previous laboratory research conducted at Oklahoma State University and in collaboration with the U.S. EPA has indicated that complex conductivity is sensitive to the presence of metallic nanoparticles under fully saturated conditions but insensitive to non-metallic particles (Joyce et al., 2012). Nonetheless, this previous study used high concentrations of nanomaterials perhaps not relevant in the environment (unless due to accumulation) and only within saturated conditions. Since the vadose zone is the potential zone of accumulation, or initial location, of nearly all contaminants that initiate at the surface, investigating the complex conductivity signatures of AgNP within the vadose zone or under partially saturated conditions is required, and useful as an aid to the detection and remediation of these potential contaminants. In this work, we report on the first results of several laboratory sand column experiments conducted to investigate the complex conductivity response of AgNPs in a partially saturated sand column designed similarly to the Cuny et al. (2015) BTC investigation. While the Cuny et al. (2015) study (among others) focused on ENM mobility under water saturated quartz sand columns, the unique experiment herein focuses on partially saturated conditions. The specific experimental treatments included: 1) a range of moisture contents (0–30%), 2) variable AgNP concentrations (0–10 mg/g), 3) two types of lithology (sand and sandy clay mixture), 4) two different fluid electrical conductivities (0.0275 and 0.1000 S/m), and 5) three grain size diameters of AgNPs (35, 90–210, and 1500–2500 nm). Our results demonstrate that complex conductivity measurements are very sensitive to the presence of AgNPs in partially saturated porous media. As such, complex conductivity could be utilized for subsurface AgNP detection, mapping, and possibly for guiding the remediation processes of such contaminants within the vadose zone.

2. Materials and methods

2.1. Silver nanoparticles (AgNPs)

AgNPs were purchased from Nanostructured and Amorphous Materials Incorporated (www.nanoamor.com) in a powder form with a purity of >99%. The AgNPs were purchased with three different particle sizes of 35, 90–210 and 1500–2500 nm and specific surface area of 30–50, 2.40–4.42 and 0.4–0.8 m^2/g, respectively.

2.2. Porous medium and pore fluid

The porous medium used for the experiments consisted of fine silica Ottawa sands (U.S. Silica Company) with a median grain diameter distribution $d_{50} = 200 \pm 10$ μm and a porosity of 0.45 ± 0.02 (calculated from the total volume of the column minus the volume of the dry sand). Kaolinite, a clay mineral (anhydrous aluminum silicate), in a powder form was also used and obtained from the Boone Pickens School of Geology, Oklahoma State University, and has an average particle size of 1.1 μm. The fluid used to partially saturate the sand column was artificial groundwater (AGW) similar to that used by Abdel Aal et al. (2009).

Two different AGW samples A and B were prepared with fluid conductivities of 0.0275 ± 0.003 S/m and 0.1000 ± 0.003 S/m, respectively. The final pH of the two AGW samples was 7.1 ± 0.01.

2.3. Sample holder and instrumentation setup

A schematic representation of the complex conductivity setup used in this study is shown in Fig. 1. The sample holder/column was constructed from polyvinyl chloride

(PVC) pipe with an inner diameter of 3.4 cm and a length of 12 cm. Four non-polarizing Ag-AgCl electrodes housed in electrolyte (agar gel mixed in 3 M concentration of KCl) filled chambers were placed 2 cm apart along the length of the column and located just outside the current flow path. The outer two electrodes were used to inject the current sinusoid and the two inner electrodes were used to record the output voltage sinusoid. The four non-polarizable electrodes (AB for the current and MN for the voltage) were connected to a dynamic signal analyzer (DSA) (National Instruments (NI) – 4461) to perform the electrical measurements between 0.1 Hz to 1 kHz at 16 equal logarithmic intervals (sensitivity of 0.1 mrad over this frequency range). An AD620 preamplifier boosted the input impedance on the voltage channel and prevented current leakage into the circuitry. The impedance magnitude $|\sigma|$ and the phase shift φ (between a measured voltage sinusoid and an impressed current sinusoid) of the sample were measured relative to a high-quality resistor. The in-phase (σ') and quadrature (σ'') parts of the sample complex conductivity Eqs. (1) and (2) were then calculated. All experiments were conducted at the same ambient temperature of 22 ± 1.0 °C.

The electrical data acquired were modeled using the well-known Cole-Cole phenomenological model (Cole and Cole, 1941) and as described by previous researchers (e.g., Pelton et al., 1978 for metallicrich rocks). From this we obtained the chargeability (m) and the time constant (τ). The chargeability is a measure of the magnitude of the polarization storage relative to the conduction loss (Lesmes and Frye, 2001; Slater et al., 2005). The normalized chargeability m_n is then obtained by multiplying the chargeability by the conductivity and is a direct measure of the polarization magnitude (interfacial polarization). The time constant τ is related to the relaxation time and is an indicator of polarizable particle size (Wu et al., 2005).

2.4. Experimental procedure

Four laboratory experiments (labeled I through IV) were conducted using complex conductivity measurements in sand columns under variable saturation conditions (Table 1).

Experiment (I) was performed to investigate the complex conductivity signature of AgNPs (90–210 nm) in fine sand at different concentrations and water saturation. The experiment was conducted by mixing a fixed amount of fine sand and AGW (Type A with EC = 0.0275 ± 0.003 S/m) with initial saturation of 0.05%. The AGW-sand mixture was then packed into the constructed column and the complex conductivity measurements were obtained from a 0.1–1000 Hz frequency range. The same procedure was repeated by using different concentrations of the same AgNPs (0, 2, 4, 6, 8, and 10 mg/g) and at different AGW saturation (0.05, 0.10, 0.15, 0.20, and 0.30).

For the next three experiments, the AgNPs concentration and water saturation were maintained at 6 mg/g and 0.15, respectively. Experiment (II) was conducted to investigate the effect of fluid conductivity on the complex conductivity response of AgNPs (90–210 nm) in fine sand with the column set up as in Experiment I. A mixture of fine sand, AGW (type A with EC = 0.0275 ± 0.003 S/m) and AgNPs was prepared, packed into the constructed column, and the complex conductivity measurements were obtained from a 0.1–1000 Hz frequency range. The same experiment was then repeated using the AGW type B (EC = 0.1000 ± 0.003 S/m).

Experiment (III) was conducted to investigate the effect of lithology on the complex conductivity response of AgNPs (90–210 nm) in fine sand and fine sand clay mixtures. A mixture of fine sand, AGW (Type A with EC = 0.0275 ± 0.003 S/m) and AgNPs was prepared, packed into the constructed column and the complex conductivity measurements were obtained from a 0.1–1000 Hz frequency range. The same experiment was repeated using fine sand +6 mg/g of clay (kaolinite). For comparison, the amount of kaolinite used was adjusted considering the difference in density between the AgNPs (10.50 g/cm^3) and Kaolinite (2.6 g/cm^3).

Experiment (IV) was performed to investigate the effect of different particle diameters of AgNPs (35, 90–210, and 1500–2500 nm) on the complex conductivity response of fine sand. We followed the procedure used in experiment (II) using AGW (Type A) but with different particle diameters of AgNPs and a fixed concentration of 6 mg/g AgNP.

3. Results and discussion

3.1. Effect of AgNP concentration and water content

The complex conductivity response from Experiment I, varying AgNP concentration, indicates that the magnitude of the quadrature conductivity increased by almost one order of magnitude as AgNP concentration increased from 0 to 10 mg/g (Fig. 2a).

In contrast, the in-phase conductivity showed negligible changes with increasing AgNP concentration (Fig. 2b). At a frequency of 10 Hz, the quadrature and in-phase conductivity showed approximately 300% and 19% change with increasing AgNPs concentration, respectively. The 10 Hz frequency was chosen as a stable, representative frequency.

Fig. 3 shows the results from Experiment I at 10 Hz as a function of different AgNPs concentrations (0, 2, 4, 6, 8, and 10 mg/g) for different water saturations (0.05, 0.10, 0.15, 0.20, and 0.30) in fine sand. The raw data are fitted with power law relationships as shown by the solid lines (the power law models are summarized in Table 2). By increasing the silver nanoparticles concentrations from 0 to 10 mg/g, the magnitude of the quadrature conductivity (σ'') increases by a percent change of 72.37, 239.90, 31.38, 381.50, and 817.57 at water saturation of 0.05, 0.10, 0.15, 0.20, and 0.30, respectively (Fig. 3a). On the other hand by increasing the AgNPs concentrations from 0 to 10 mg/g, the in-phase conductivity (σ') magnitude showed only a small percent change of −35.85, 38.67, 19.67, 17.98 and 25.6 at water saturation of 0.05, 0.10, 0.15, 0.20, and 0.30, respectively (Fig. 3b).

Table 2 summarizes the power law fitted equations and correlation coefficients (R^2) for quadrature (σ'') and in-phase (σ') conductivity components at 10 Hz as a function of different AgNPs concentrations for different water saturation in fine sand. The power law exponents for the quadrature fitted equations increase with increasing the water saturation at different AgNPs concentrations with very good correlation coefficient ($0.80 <= R^2 \geq 0.97$).

As a result, these power law fitted equations can be used to estimate the AgNPs concentration from the measured quadrature conductivity at different water saturations. The power law exponents for the in-phase fitted equations do not show a clear trend with increasing the water saturation at different AgNPs concentrations with poor correlation coefficients ($0.21 <= R^2 < 0.94$). Very low water saturation (0.05) displays the best correlation coefficient of (0.94) for the in-phase power law models. These results suggest there is a linear relationship between the quadrature conductivity and the volume content of AgNPs in the porous media. Thus, we suggest that the increase in the magnitude of the quadrature conductivity resulted from the increase in the amount of metallic minerals within the pore volume. Several studies have demonstrated that increasing the amount of metallic minerals within the pore volume increases the magnitude of the polarization response (i.e., the quadrature component of the complex conductivity) (e.g. Slater et al., 2005, 2006; Weller et al., 2010; Abdel Aal et al., 2014; Hupfer et al., 2015). In addition, a relationship between the percentage of metallic minerals and the magnitude of the complex conductivity response has been well documented (Pelton et al., 1978; Vanhala and Peltoniemi, 1992; Seigel et al., 1997; Bigalke and Junge, 1999; Revil et al., 2015a,b). In contrast, the smaller magnitude change observed from the in-phase conductivity is not surprising as the in-phase conductivity component is largely dependent on the conductivity of the electrolytic fluid and the amount of fluid in the pore space (Slater et al., 2005; Slater and Glaser, 2003; Schmutz et al., 2010). Fig. 3b demonstrates this clearly as we observe an increase in the in-phase conductivity with increasing saturation but smaller changes with increasing AgNPs concentration. Although Ag is an electronic conductor, significant contributions of electronic conduction to the measured in-phase conductivity is possible when grain to grain contact of the AgNP results in a continuous electronic conduction path (Abdel Aal et al., 2014). However, the minimal changes in the in-phase conductivity suggest a breakdown of such a connection which diminished any contribution of electronic conduction of the conductive AgNP.

Currently, the typical concentrations for ENM in the environment are unknown, as these are difficult to determine and rely on modeling studies and analytical measurements. Although we have demonstrated that geophysical measurements such as complex conductivity can detect the presence of metallic nanoparticles in column experiments under partially saturated conditions, the question remains whether these measurements can be used to detect ENM in concentrations that might be found in the environment. To answer this question, we looked into the literature for answers in order to determine whether the concentrations 2–10 mg/g are environmentally relevant. Gottschalk et al. (2013) provide concentration ranges from 10^{-7} mg/L to 0.1 mg/L for most ENM with AgNPs ranges from ~ 10^{-7} mg/L to 0.1 mg/L; however the authors admit that there is great variability of up to 1000 mg/L for estimates of AgNP. Even though the concentrations used in the present study are much higher than values documented in the Gottschalk et al. (2013) study, we find

that our experimental concentrations are consistent with values used in many other ENM experiments in the literature (e.g., Chowdhury et al., 2011 (0.8 mg/g); Medvedeva et al., 2013 (1 mg/g); Tang and Lo, 2013; (5 mg/g); Zhang, 2003 (6.25 mg/g)). Additionally, the Benn et al. (2010) study found AgNPs products washed in tap water for 1 h to release AgNPs concentrations ranging from <0.0002 to 0.046 mg per g of product mass. This experiment went further and simulated the release of AgNPs into landfills via four likely products and found AgNPs concentrations to range from 0.002 to 0.054 mg per g of product mass over a 24 h release duration. Importantly the authors note that leaching concentrations would likely be higher under real-world conditions due to higher pH, higher temperatures, mechanical stress and the presence of oxidants. Generally, the environment will serve as a sink for the accumulation of AgNPs, where the concentration is difficult to determine due to environmental chemistry variability, agglomeration, and time (Benn et al., 2010). Furthermore, Dror et al. (2015) show AgNP concentration depth profiles range from approximately 5.39 mg/g to almost 107 mg/g over a variety of clay content, DOC, extractable Al, and pH soils.

3.2. Effect of ionic strength

Fig. 4 shows the results from Experiment II for 15% partially saturated fine sand with fluid conductivities of A (0.0275 S/m) and B (0.1 S/m) in the absence (open symbols) and presence (filled symbols) of AgNPs (at a concentration of 6 mg/g).

In the absence of AgNPs (open symbols), the partially saturated sand with lower fluid conductivity A (0.0275 S/m) shows higher average quadrature conductivity (σ'') magnitude of 1.79×10^{-6} S/m compared to the partially saturated sand with higher fluid conductivity B (0.1 S/m) of 1.57×10^{-6} S/m (Fig. 4a). On the other hand, the in-phase conductivity (σ') displays a lower average magnitude of 1.07×10^{-3} S/m for the partially saturated sand with lower fluid conductivity A (0.0275 S/m) compared to the partially saturated sand with higher fluid conductivity B (0.1 S/m) with an average $\sigma' = 1.71 \times 10^{-3}$ S/m) (Fig. 4b). The addition of the AgNPs increased the magnitude of the average quadrature conductivity (σ'') to (4.28×10^{-6} S/m) and (5.15×10^{-6} S/m) (Fig. 4a) and the average in-phase conductivity (σ') to (1.13×10^{-3} S/m) and 1.74×10^{-3} S/m) for the partially saturated sand with fluid conductivity A (0.0275 S/m) and B (0.1 S/m) (Fig. 4b), respectively. Overall, we observe an increase in the quadrature conductivity due to the addition of AgNPs and an expected increase in the real conductivity within the highest fluid conductivity (B-0.1 S/m). These results suggest that ionic strength affects the complex conductivity response of AgNPs since both the Type A and Type B fluids showed increases with AgNP. The quadrature response is enhanced in the presence of higher pore fluid conductivity probably due to the effect of higher ionic charge density in the highest fluid conductivity fluid (B-0.1 S/m).

3.3. Effect of lithology

Since most soils and near surface sediments are heterogeneous, we initially investigated heterogeneity by adding kaolinite to our sand mixtures. Fig. 5 shows the Experiment III results of the complex conductivity measurements for 15% partially saturated fine sand (FS) and fine sand (FS) + 6 mg/g clay in the absence (open symbols) and presence (filled symbols) of AgNPs with a concentration of 6 mg/g are shown in Fig. 5. In the absence of

AgNPs, the partially saturated fine sand (FS) showed average quadrature conductivity (σ'') magnitude of 1.79×10^{-6} S/m, expectedly lower than the partially saturated fine sand with clay (FS + Clay) of 7.672×10^{-6} S/m (Fig. 5a) due to the known quadrature response to clays. Alternatively, the in-phase conductivity (σ') displays a lower average magnitude of 1.07×10^{-3} S/m for the partially saturated fine sand (FS) compared to the partially saturated fine sand with clay (FS + Clay) of 1.79×10^{-3} S/m (Fig. 5b). The addition of 6 mg/g of the AgNPs increases the magnitude of the quadrature conductivity (σ'') to 4.28×10^{-6} S/m and 1.30×10^{-5} S/m (Fig. 5a) and the in-phase conductivity (σ') to 1.13×10^{-3} S/m and 1.83×10^{-3} S/m (Fig. 5b) for the partially saturated find sand (FS) and fine sand with clay (FS + Clay), respectively. The overall increase in the complex conductivity parameters due to the addition of AgNPs is higher for the fine sand with clay. Clays are known to have a large surface area and high cation exchange capacity; hence, they are highly polarizable (e.g., Revil, 2013). Thus, the addition of clay to sand mixtures dramatically increased the quadrature conductivity as observed in Fig. 5a. Accordingly, as was previously observed by Abdel Aal et al. (2014), the effect of the two conductive minerals (in the case of the present study, AgNPs and clays) increased the volume fraction of the polarized particles and; therefore, enhanced the total polarization, which is consistent with a new model by Revil et al. (2015a,b) that showed that in the presence of a polarizable background (e.g., a clayey matrix), the total polarization is additive (essentially that of the metallic particles plus the polarizable background). Since clay minerals are common components of soils and sediments. Therefore, the detection of AgNPs and other metallic ENM are likely to be enhanced in clayey soils. The magnitude of the in-phase response is very minimal due to these changes and largely indistinguishable from the response without AgNPs.

3.4. Effect of AgNPs particle size

Fig. 6 shows the Experiment IV results of complex conductivity measurements from 15% partially saturated fine sand with 6 mg/g AgNPs with concentration at different particle size diameters (35, 90–210, and 1500–2500 nm). The average quadrature conductivity (σ'') magnitude increased from 1.52×10^{-6} S/m to 4.06×10^{-6} S/m and 1.37×10^{-5} S/m by decreasing the AgNPs grain size diameter from 1500 to 2500 nm to 90–210 nm and 35 nm, respectively (Fig. 6a). While not as large, the average in-phase conductivity (σ') magnitude increases from 1.02×10^{-3} S/m to 1.07×10^{-3} S/m and 1.51×10^{-3} S/m by decreasing the AgNPs grain size diameter from 1500 to 2500 nm to 90–210 nm and 35 nm, respectively (Fig. 6b). The observed increase in the average quadrature conductivity (σ'') magnitude accompanying the decreasing in the AgNPs grain size diameter is more pronounced at frequencies higher than 10 Hz (Fig. 6a) and greater than the increase in the average magnitude of the in-phase conductivity (σ') (Fig. 6b).

Fig. 7 summarizes the relationship between the modeled parameters m_n and τ and our results presented in Figs. 2-6. The variation of both m_n and τ is consistent with the behavior of the spectra shown on Figs. 2a, 3a, 4a, 5a, and 6a. We observe an increase in both m_n and τ with increasing AgNP concentration and water content (Fig. 7a1, a2) and interpret this to be due to the increase surface area resulting from the higher concentration of AgNP. Fig. 7b1 and b2 displays the effect of salinity and the presence of AgNP. Both the normalized chargeability and relaxation are highest for B + AgNP, next with A + AgNP and equally

lowest without AgNP for both pore fluids, A and B. So, the presence of AgNP increases the chargeability regardless of the fluid chemistry; suggesting this is a surface charge storage response mechanism and while the presence of more saline pore fluid increases the magnitude of each parameter, the addition of AgNP and its surface characteristics and surface area effect is the largest contributor to both m_n and τ. Next, Fig. 7c1 and c2 displays the effect of lithology. We observe that chargeability is directly proportional to lithology (Fig. 7c1) and the more surface area as fine sand + clay + AgNP exhibits the highest chargeability. However, the relaxation response (Fig. 7c2) due to lithology is not as linear as chargeability. Here the relaxation response is similar to the effect of fluid chemistry, where the presence of AgNP results in the higher responses, with the highest relaxation occurring when clay is present, which is likely due to the surface area and surface charge of clay dominating the relaxation response. Lastly, Fig. 7d1 and d2 examines the effect of AgNP grain size diameter and the Cole-Cole parameters. We observe that chargeability is inversely proportional to the size of AgNP (Fig. 7d1), which is understood as the effect of surface area to chargeability and is comparable to sand-metal mixtures (Pelton et al., 1978; Gurin et al., 2013, 2015; Slater et al., 2006; Hupfer et al., 2015). Alternatively, relaxation (Fig. 7d2) is directly proportional to the size of AgNP, where the largest AgNP has the largest relaxation response and supports the understanding of the τ dependence on grain size and our results are consistent with those of other researchers (e.g. Gurin et al., 2013; Hupfer et al., 2015).

Several studies have demonstrated that the surface area per pore volume of the porous material or specific surface area exerts a major control on the polarization and is directly related to the quadrature conductivity (e.g. Slater et al., 2005, 2006; Weller et al., 2010; Gurin et al., 2013, 2015; Hupfer et al., 2015). In our study, the specific surface area of the 35 nm particle size is 30–50 m^2/g, higher than the 0.4–0.8 m^2/g of the 1500–2500 nm particle size and this particle size also shows the highest magnitude response. Furthermore, Dror et al. (2015) show that ENM deposition to the solid soil phase is similar to colloid attachment efficiency where ENMs are deposited on soil solid surfaces from the interaction with natural clays, humic substances, and organic matter (Dror et al., 2015). This accumulation of ENMs on the solid surface is likely the result of adhesion, pore structure, and hydrodynamic effects (Torkzaban et al., 2007; Bradford and Torkzaban, 2008) and is shown diagrammatically in Fig. 8. Arab and Pourafshary (2013) suggest that ENM deposition on soil surfaces leads to the alteration of the soil surface charge. From a complex conductivity perspective, this suggests the surface alterations of the native soil solids by ENMs would likely alter the electrical double layer (Dror et al., 2015) and be realized in the complex conductivity quadrature response, which is precisely what we observe. Dror et al. (2015) importantly state that the potential of ENMs on solid soil particles to alter soil properties is specific to the type of soil and the type of ENM; thus, highlighting the site specific nature of field detection measurements. For instance, positively charged ENMs would preferable attach to negatively charged soil particles, or visa-versa.

Additional work by Ng and Coo (2014) shows a 30–45% hydraulic conductivity reduction for clays with Al_2O_3 and CuO ENMs as compared to clays not treated with ENMs. Further additions of ENMs reduced the hydraulic conductivity due to ENM pore clogging, perhaps due to ENM aggregates (Dror et al., 2015). All of these ENM induced physical alterations

would also be measureable with complex conductivity due to its sensitivity to grain surface chemistry, morphology, and alterations.

While the results presented herein do not determine hydraulic conductivity, a clear relationship exists between matrix size, matrix saturation, AgNP particle size, and AgNP concentration to the complex conductivity response. Future experiments may include correlation to hydraulic conductivity.

4. Conclusions

The small size of metallic environmental nanomaterials, high surface area to volume ratio, and electrical conductivity make metallic environmental nanomaterials ideal targets for detection with low frequency electrical geophysical techniques, such as complex conductivity. We have demonstrated that the complex conductivity method is very sensitive to the presence of nanoparticles within experimental vadose zone conditions. Under partially saturated conditions, the quadrature conductivity magnitude is enhanced in the presence of residual soil moisture, high ionic strength of the pore fluids, clays, and most importantly the high surface area of the metallic nanoparticles. In addition, the strong dependence of the quadrature conductivity on the volumetric metal content suggests that this parameter can be used to quantify concentrations of metallic environmental nanomaterials in the environment; however, more studies are required to confirm this proposition. We find that the in-phase component, which is strongly dependent on electrolytic conductivity and comparable to direct current resistivity techniques, is not useful for the detection of environmental nanomaterials.

In an attempt to minimize the variables influencing the complex conductivity response, we have presented experiments that decouple the influence of saturation, nanoparticle size, ionic strength, and the matrix grain size on the complex conductivity response to AgNPs in porous media. Of course, actual environmental conditions are likely more heterogeneous and anisotropic thereby compounding these variables and making the complex conductivity more difficult to interpret. Nonetheless, the above results provide some baseline measurements from which more complex experiments can be built upon to investigate both heterogeneity and coupled processes.

The results from our study may only be experimental and laboratory controlled, yet as the demand to develop techniques to detect the presence and transport of nanoparticles in the subsurface increases, these results could potentially be used in guiding the remediation processes of such contaminants or useful for indirect or direct detection, characterization, or mapping. Future studies will address the fate and transport of environmental nanomaterials using electrical geophysical techniques under more environmentally relevant conditions (e.g., saturation, salinity, temperature, pH).

Acknowledgment

The United States Environmental Protection Agency through its Office of Research and Development student services contract # EP09D000553 partially funded and collaborated in this research. It has been subjected to Agency review and approved for publication. Mention of trade names or commercial products does not constitute

endorsement or recommendation for use. GA was funded by the office of the Dean, College of Arts and Sciences, Oklahoma State University. This is the Boone Pickens School of Geology Contribution 2016-45.

References

Abdel Aal GZ, Atekwana E, Radzikowski S, Rossbach S, 2009. Effect of bacterial adsorption on low frequency electrical properties of clean quartz sands and iron-oxide coated sands. Geophys. Res. Lett 36:L04403. 10.1029/2008GL036196.

Abdel Aal GZ, Atekwana EA, Revil A, 2014. Geophysical signatures of disseminated iron minerals: a proxy for understanding subsurface biophysicochemical processes. J. Geophys. Res. Biogeosci 119. 10.1002/2014JG002659.

Arab and Pourafshary, 2013. Nanoparticles-assisted surface charge modification of the porous medium to treat colloidal particles migration induced by low salinity water flooding. Colloids Surf. A Physicochem. Eng. Asp 436:803–814. 10.1016/j.colsurfa.2013.08.022.

Asharani PV, Wu YL, Gong ZY, Valiyaveettil S, 2008. Toxicity of silver nanoparticles in zebrafish models. Nanotechnology (19:255102). [PubMed: 21828644]

Benn T, Cavanagh B, Hristovski K, Posner JD, Westerhoff P, 2010. The release of nanosilver from consumer products used in the home. J. Environ. Qual 39:1875. 10.2134/jeq2009.0363. [PubMed: 21284285]

Benoit R, Wilkinson KJ, Sauvé S, 2013. Partitioning of silver and chemical speciation of free Ag in soils amended with nanoparticles. Chem. Cent. J 7:75. 10.1186/1752-153X-7-75. [PubMed: 23617903]

Bigalke, Junge, 1999. Using evidence of non-linear induced polarization for detecting extended ore mineralizations. Geophys. J. Int 137, 516–520.

Blaser SA, Scheringer M, MacLeod M, Hungerbuhler K, 2008. Estimation of cumulative aquatic exposure and risk due to silver: contribution of nanofunctionalized plastics and textiles. Sci. Total Environ 390, 396–409. [PubMed: 18031795]

Bouchard D, Ma X, Isaacson C, 2009. Colloidal properties of aqueous fullerenes: isoelectric points and aggregation kinetics of C_{60} and C_{60} derivatives. Environ. Sci. Technol 43, 6597–6603. [PubMed: 19764223]

Boxall AB, Tiede K, Chaudhry Q, 2007. Engineered nanomaterials in soils and water: how do they behave and could they pose a risk to human health? Nanomedicine 2, 919–927. [PubMed: 18095854]

Bradford SA, Torkzaban S, 2008. Colloid transport and retention in unsaturated porous media: a review of interface-, collector-, and pore-scale processes and models. Vadose Zone J. 7:667. 10.2136/vzj2007.0092.

Braunschweig J, Bosch J, Meckenstock RU, 2013. Iron oxide nanoparticles in geomicrobiology: from biogeochemistry to bioremediation. New Biotechnol. 30, 793–802.

Busch J, Meiner T, Potthoff A, Bleyl S, Georgi A, Mackenzie K, Oswald SE, 2015. A field investigation on transport of carbon-supported nanoscale zero-valent iron (nZVI) in groundwater. J. Contam. Hydrol 181:59–68. 10.1016/j.jconhyd.2015.03.009. [PubMed: 25864966]

Cai L, Zhu LJ, Hou Y, Tong M, Kim H, 2015. Influence of gravity on transport and retention of representative engineered nanoparticles in quartz sand. J. Contam. Hydrol 181:153–160. 10.1016/j.jconhyd.2015.02.005. [PubMed: 25728046]

Chen, Elimelech, 2008. Interaction of fullerene (C_{60}) with humic acid and alginate coated silica surfaces: measurements, mechanisms, and environmental implications. Environ. Sci. Technol 42:7607–7614. 10.1021/es9012062. [PubMed: 18983082]

Chowdhury I, Hong Y, Honda RJ, Walker SL, 2011. Mechanisms of TiO_2 nanoparticle transport in porous media: role of solution chemistry, nanoparticle concentration, and flowrate. J. Colloid Interface Sci 360, 548–555. [PubMed: 21640358]

Cole KS, Cole RH, 1941. Dispersion and absorption in dielectrics I. Alternating current characteristics. J. Chem. Phys 9:341. 10.1063/1.1750906.

Cornelis G, Pang L, Doolette C, Kirby JK, McLaughlin MJ, 2013. Transport of silver nanoparticles in saturated columns of natural soils. Sci, Total Environ. 463–464:120–130. 10.1016/j.scitotenv.2013.05.089.

Cornelis G, Hund-Rinke K, Kuhlbusch T, van den Brink N, Nickel C, 2014. Fate and bioavailability of engineered nanoparticles in soils: a review. Crit. Rev. Environ. Sci. Technol 44:2720–2764. 10.1080/10643389.2013.829767.

Cuny L, Herrling MP, Guthausen G, Horn H, Delay M, 2015. Magnetic resonance imaging reveals detailed spatial and temporal distribution of iron-based nanoparticles transported through water-saturated porous media. J. Contam. Hydrol 182:51–62. 10.1016/j.jconhyd.2015.08.005. [PubMed: 26335945]

Delay, Frimmel F, 2012. Nanoparticles in aquatic systems. Anal. Bioanal. Chem 402, 583–592. [PubMed: 22038580]

Dror I, Yaron B, Berkowitz B, 2015. Abiotic soil changes induced by engineered nanomaterials: a critical review. J. Contam. Hydrol 181:3–16. 10.1016/j.jconhyd.2015.04.004. [PubMed: 25913535]

Gerloff K, Fenoglio I, Carella E, Kolling J, Albrecht C, Boots AW, Förster I, Schins RP, 2012. Distinctive toxicity of TiO_2 rutile/anatase mixed phase nanoparticles on Caco-2 cells. Chem. Res. Toxicol 25, 646–655. [PubMed: 22263745]

Glover RD, Miller JM, Hutchison JE, 2011. Generation of metal nanoparticles from silver and copper objects: nanoparticle dynamics on surfaces and potential sources of nanoparticles in the environment. ACS Nano 5, 8950–8957. [PubMed: 21985489]

Gottschalk F, Kost E, Nowack B, 2013. Engineered nanomaterials in water and soils: a risk quantification based on probabilistic exposure and effect modeling. Environ. Toxicol. Chem 32:1278–1287. 10.1002/etc.2177 (32(6):1278–87). [PubMed: 23418073]

Gurin G, Tarasov A, Ilyin Y, Titov K, 2013. Time domain spectral induced polarization of disseminated electronic conductors: laboratory data analysis through the Debye decomposition approach. J. Appl. Geophys 98:44–53. 10.1016/j.jappgeo.2013.07.008.

Gurin G, Titov K, Ilyin Y, Tarasov A, 2015. Induced polarization of disseminated electronically conductive minerals: a semi-empirical model. Geophys. J. Int 200, 1555–1565.

Handy RD, Own R, Valsami-Jones E, 2008. The ecotoxicology of nanoparticles and nanomaterials: current status, knowledge gaps, challenges, and future needs. Ecotoxicology 17:315–325. 10.1007/s10646-008-0206-0. [PubMed: 18408994]

Hosseini SM, Tosco T, 2013. Transport and retention of high concentrated nano-Fe/Cu particles through highly flow-rated packed sand column. Water Res. 47:326–338. 10.1016/j.watres.2012.10.002. [PubMed: 23141767]

Hupfer S, Martin T, Weller A, Günther T, Kuhn K, Djotsa V, Ngninjio V, Noell U, 2016. Polarization effects of unconsolidated sulphide-sand-mixtures. J. Appl. Geophys 135, 456–465.

Hussain SM, Warheit DB, Ng SP, Comfort KK, Grabinski CM, Braydich-Stolle LK, 2015. At the crossroads of nanotoxicology in vitro: past achievements and current challenges. Toxicol. Sci 147:5–16. 10.1093/toxsci/kfv106. [PubMed: 26310852]

Ivanova, Zamborini, 2009. Size-dependent electrochemical oxidation of silver nanoparticles. J. Am. Chem. Soc 132:70–72. 10.1021/ja908780g.

Joyce RA, Glaser DR, Werkema DD Jr., Atekwana EA, 2012. Spectral induced polarization response to nanoparticles in a saturated sand matrix. J. Appl. Geophys 77. 10.1016/j.jappgeo.2011.11.009, pp. 63–71.

Kabashin A, Meunier VM, Kingston CJ, Luong HT, 2003. Fabrication and characterization of gold nanoparticles by femtosecond laser ablation in an aqueous solution of cyclodextrins. J. Phys. Chem. B 1074, 527–4531.

Kim JS, Kuk E, Yu KN, Kim J-H, Park SJ, Lee HJ, Kim SH, Park YK, Park YH, Hwang C-Y, 2007. Antimicrobial effects of silver nanoparticles. Nanomed. Nanotechnol. Biol. Med 3, 95–101.

Klaine SJ, Alvarez PJJ, Batley GE, Fernandes TF, Handy RD, Lyon DY, Mahendra S, McLaughlin MJ, Lead JR, 2008. Nanomaterials in the environment: behavior, fate, bioavailability and effects. Environ. Toxicol. Chem 27, 1825–1851. [PubMed: 19086204]

Lesmes, Frye, 2001. Influence of pore fluid chemistry on the complex conductivity and induced polarization responses of Berea sandstone. J. Geophys. Res 106:B3, 4079–4090.

Luque-Garcia JL, Sanchez-Dý'az R, Lopez-Heras I, Camara C, Martin P, 2013. Bioanalytical strategies for in vitro and in vivo evaluation of the toxicity induced by metallic nanoparticles. Trends Anal. Chem 43, 254–268.

Ma X, Geiser-Lee J, Deng Y, Kolmakov A, 2010. Interactions between engineered nanoparticles (ENPs) and plants: phytotoxicity, uptake and accumulation. Sci. Total Environ 408, 3053–3061. [PubMed: 20435342]

Mansoor N, Slater L, 2007. On the relationship between iron concentration and induced polarization in marsh soils. Geophysics 72 (1):A1–A5. 10.1190/1.2374853.

Medvedeva I, Bakhteeva J, Zhakov S, Revvo A, Bysov I, Uimin M, Yermakov A, Mysik A, 2013. Sedimentation and aggregation of magnetite nanoparticles in water by a gradient magnetic field. J. Nanopart. Res 15:2054. 10.1007/s11051-013-2054-y.

Navarro E, Piccapietra F, Wagner B, Marconi F, Kaegi R, Odzak N, Sigg L, Behra R, 2008. Toxicity of silver nanoparticles to *Chlamydomonas reinhardtii*. Environ. Sci. Technol 42, 8959–8964. [PubMed: 19192825]

Ng, Coo, 2014. Hydraulic conductivity of clay mixed with nanomaterials. Can. Geotech. J 52:808–811. 10.1139/cgj-2014-0313.

Ntarlagiannis D, Williams KH, Slater L, Hubbard S, 2005. Low frequency electrical response to microbial induced sulfide precipitation. J. Geophys. Res 110:G02009. 10.1029/2005JG0000.

Pelton WH, Ward SH, Hallof PG, Sill WR, Nelson PH, 1978. Mineral discrimination and removal of inductive coupling with multifrequency IP. Geophysics 43, 588–609.

Prédélus D, Coutinho AP, Lassabatere L, Bien LB, Winiarski T, Angulo-Jaramillo R, 2015. Combined effect of capillary barrier and layered slope on water, solute and nanoparticle transfer in an unsaturated soil at lysimeter scale. J. Contam. Hydrol 181:69–81. 10.1016/j.jconhyd.2015.06.008. [PubMed: 26184062]

Rakshit S, Sarkar D, Elzinga EJ, Punamiya P, Datta R, 2013. Mechanisms of ciprofloxacin removal by nano-sized magnetite. J. Hazard. Mater:246–247 10.1016/j.jhazmat.2012.12.032.

Revil A, 2013. On charge accumulations in heterogeneous porous materials under the influence of an electrical field. Geophysics 78:D271–D291. 10.1190/geo2012-0503.1.

Revil A, Glover P, 1998. Nature of surface electrical conductivity in natural sands, sand-stones, and clays. Geophys. Res. Lett 25, 691–694.

Revil A, Karaoulis M, Johnson T, Kemna A, 2012. Review: some low frequency electrical methods for subsurface characterization and monitoring in hydrogeology. Hydrogeol. J 20 (4):617–658. 10.1007/s10040-011-0819-x.

Revil A, Florsch N, Mao D, 2015a. Induced polarization response of porous media with metallic particles — part 1: a theory for disseminated semiconductors. Geophysics 80. 10.1190/geo2014-0577.1.

Revil A, Abdel Aal GZ, Atekwana EA, Deqiang M, Florsch N, 2015b. Induced polarization response of porous media with metallic particles. 2. Comparison with a broad database of experimental data. Geophysics 80:D539–D552. 10.1190/GEO2014-0578.1.

Schmutz M, Revil A, Vaudelet P, Batzle M, Femenia Vinao P, Werkema DD Jr., 2010. Influence of oil saturation upon spectral induced polarization of oil-bearing sands. Geophys. J. Int 1365–246:04751. 10.1111/j1365-246x.

Seigel HO, Vanhala H, Sheard SN, 1997. Some case histories of source discrimination using time-domain spectral IP. Geophysics 62, 1394–1408.

Shi Z, Fan D, Johnson RL, Tratnyek PG, Nurmi Y, Wu Y, Williams KH, 2015. Methods for characterizing the fate and effects of nanozerovalent iron during groundwater remediation. J. Contam. Hydrol 181:17–35. 10.1016/j.jconhyd.2015.03.004. [PubMed: 25841976]

Slater, Glaser D, 2003. Controls on induced polarization in sandy unconsolidated sediments and application to aquifer characterization. Geophyiscs 68 (5):1547–1558. 10.1190/1.1620628.

Slater LD, Choi J, Wu Y, 2005. Electrical properties of iron-sand columns: implications for induced polarization investigation and performance monitoring of iron-wall barriers. Geophysics 70, G87–G94.

Slater L, Ntarlagiannis D, Wishart D, 2006. On the relationship between induced polarization and surface area in metal-sand and clay-sand mixtures. Geophyiscs 71, A1–A5.

Tang Lo, 2013. Magnetic nanoparticles: essential factors for sustainable environmental applications. Water Res. 47, 2613–2632. [PubMed: 23515106]

Thakkar KN, Mhatre SS, Parikh RY, 2010. Biological synthesis of metallic nanoparticles. Nanomedicine 6, 257–262. [PubMed: 19616126]

Torkzaban S, Bradford SA, Walker SL, 2007. Resolving the coupled effects of hydrodynamics and DLVO forces on colloid attachment in porous media. Langmuir 23:9652–9660. 10.1021/la700995e. [PubMed: 17705511]

Tosco T, Papini MP, Viggi CC, Sethi R, 2014. Nanoscale zerovalent iron particles for groundwater remediation, a review. J. Clean. Prod 77:10–21. 10.1016/j.jclepro.2013.12.026.

Vance ME, Kuiken T, Vejerano EP, McGinnis SP, Hochella MF, Rejeski D, Hull MS, 2015. Nanotechnology in the real world: redeveloping the nanomaterial consumer products inventory. Beilstein J. Nanotechnol 6:1769–1780. 10.3762/bjnano.6.181. [PubMed: 26425429]

Vanhala, Peltoniemi, 1992. Spectral IP studies of Finnish ore prospects. Geophyiscs 57, 1545–1555.

Waxman, Smits, 1968. Electrical conductivities in oil-bearing shaly sands. Soc. Pet. Eng. J 8 (2), 107–122.

Weller A, Nordsiek S, Debschütz W, 2010. Estimating permeability of sandstone samples by nuclear magnetic resonance and spectral-induced polarization. Geophyiscs 75 (6), E215–E226.

Williams KH, Ntarlagiannis D, Slater LD, Dohnalkova A, Hubbard SS, Banfield JF, 2005. Geophysical imaging of stimulated microbial biomineralization. Environ. Sci. Technol 39, 7592–7600. [PubMed: 16245832]

Williams KH, Kemna A, Wilkins MJ, Druhan J, Arntzen E, N'Guessan AL, Long PE, Hubbard SS, Banfield JF, 2009. Geophysical monitoring of coupled microbial and geochemical processes during stimulated subsurface bioremediation. Environ. Sci. Technol 43, 6717–6723. [PubMed: 19764240]

Wong J, 1979. An electrochemical model of the induced polarization phenomenon in disseminated sulfide ores. Geophyiscs 44, 1245–1265.

Wu Y, Slater LD, Korte N, 2005. Effect of precipitation on low frequency electrical properties of zerovalent iron columns. Environ. Sci. Technol 39, 9197–9204. [PubMed: 16382942]

Wu Y, Slater LD, Versteeg R, LaBrecque D, 2009. Calcite precipitation dominates the electrical signatures of zero valent iron column under simulated field conditions. J. Contam. Hydrol 106, 131–143. [PubMed: 19342119]

Zhang W-X, 2003. Nanoscale iron particles for environmental remediation: an overview. J. Nano. Part. Res 5, 323–332.

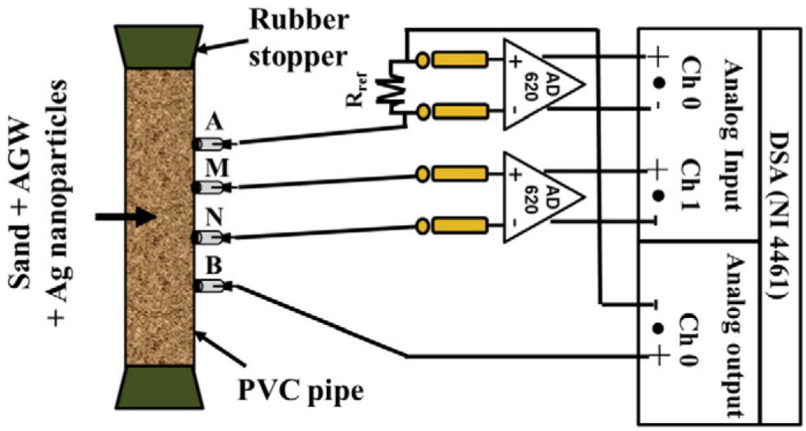

Fig. 1.

Schematic of column setup and instrumentation used in the complex conductivity measurements. The complex conductivity measurements are obtained using a dynamic signal analyzer (DSA) (National Instruments (NI) – 4461) and AD620 preamplifier to boost the input impedance on the voltage channel and prevented current leakage into the circuitry (the system sensitivity is <0.1 mrad at frequencies below 100 Hz).

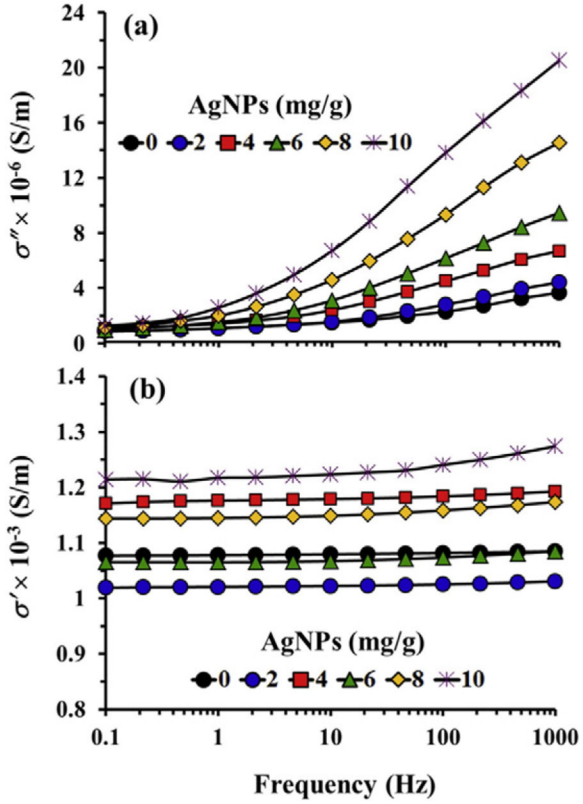

Fig. 2.

Experiment I AgNP concentration changes results: (a) quadrature conductivity (σ''), and (b) in-phase conductivity (σ') of different silver nanoparticles (AgNPs) concentration in 15% partially saturated fine sand. The quadrature conductivity (σ'') magnitude increases with increasing the silver nanoparticles concentrations whereas the in-phase conductivity (σ') magnitude shows smaller changes.

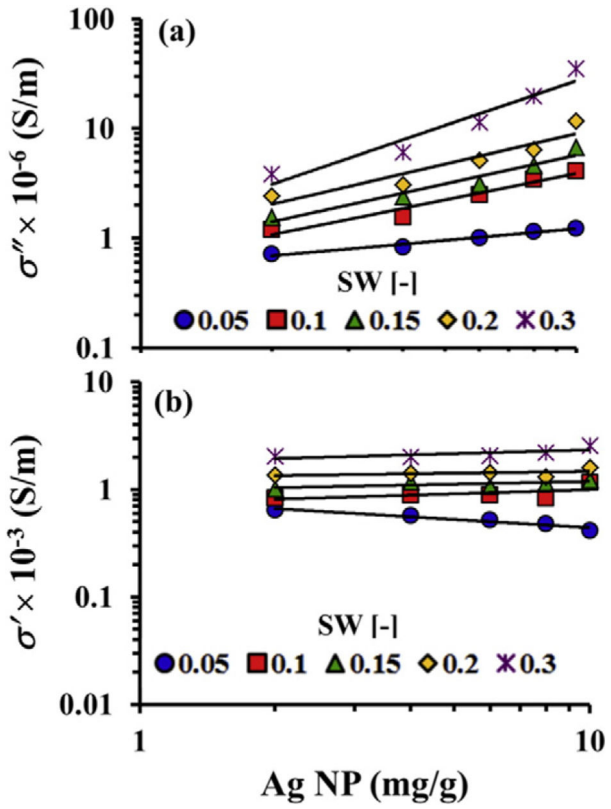

Fig. 3.

Experiment I AgNP and Sw variability results; (a) quadrature conductivity (σ''), and (b) in-phase conductivity (σ') at 10 Hz as a function of different silver nanoparticles (AgNPs) concentrations (0, 2, 4, 6, 8, and 10 mg/g) for different water saturation (0.05, 0.10, 0.15, 0.20, and 0.30) in fine sand. The data points are fitted with power law relationships as shown by the solid lines (power law models are summarized in Table 2). At different water saturation, the quadrature conductivity (σ'') magnitude increases with increasing the silver nanoparticles concentrations. The in-phase conductivity (σ') magnitude increases with increasing water saturation with insignificant change with increasing the silver nanoparticles concentrations.

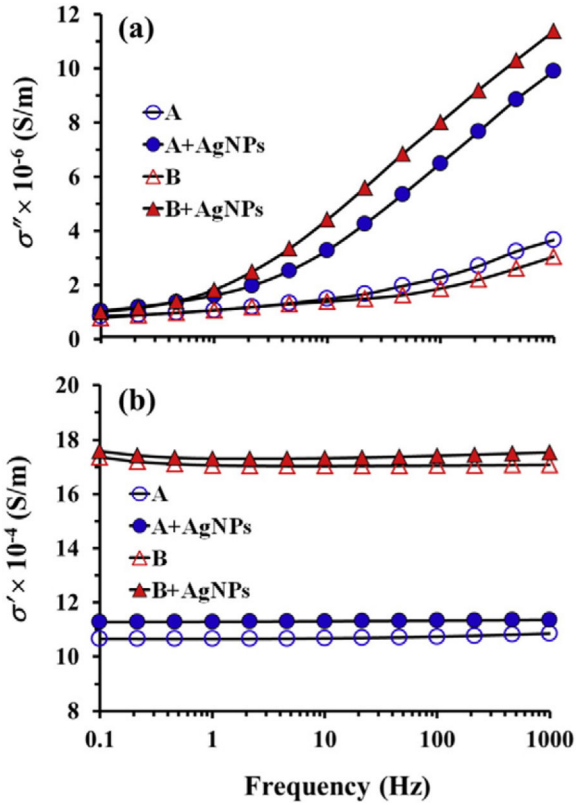

Fig. 4.

Experiment II, pore fluid conductivity variability results; (a) quadrature conductivity (σ''), and (b) in-phase conductivity (σ') for 15% partially saturated fine sand with fluid conductivities of A (0.0275 S/m) and B (0.1000 S/m) in the absence (open symbols) and presence (filled symbols) of silver nanoparticles (AgNPs with concentration of 6 mg/g). The addition of the silver nanoparticles increases the magnitude of all parameters being higher for the highest fluid conductivity (B-0.1000 S/m). Note the scales of (a) and (b) are now the same.

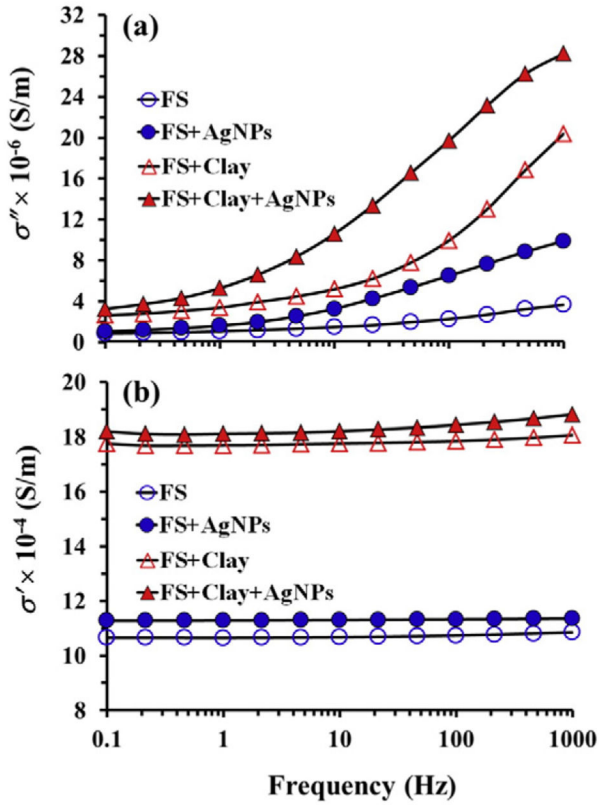

Fig. 5.

Experiment III results from lithology variability; (a) quadrature conductivity (σ''), and (b) in-phase conductivity (σ') for 15% partially saturated fine sand (FS) and fine sand + 6 mg/g clay in the absence (open symbols) and presence (filled symbols) of silver nanoparticles (AgNPs with concentration of 6 mg/g). The addition of the silver nanoparticles increases the magnitude of all parameters being higher for the fine sand (FS) + clay + AgNPs than fine sand (FS) + AgNPs.

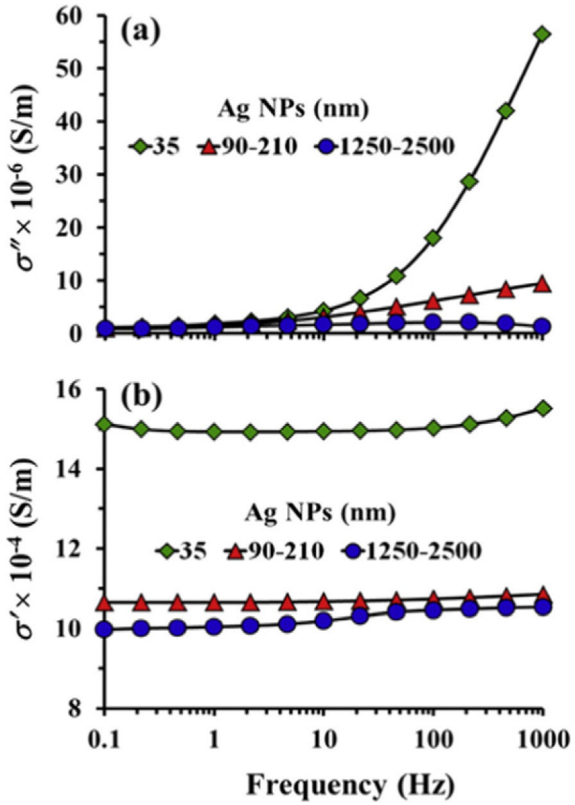

Fig. 6.

Experiment IV results from AgNP particle size variability; (a) quadrature conductivity (σ''), and (b) in-phase conductivity (σ') for 15% partially saturated fine sand (FS) and silver nanoparticles (AgNPs with concentration of 6 mg/g) with different grain size diameters (35, 90–210, and 1500–2500 nm). The magnitudes of all parameters increase with decreasing grain size diameters of AgNPs.

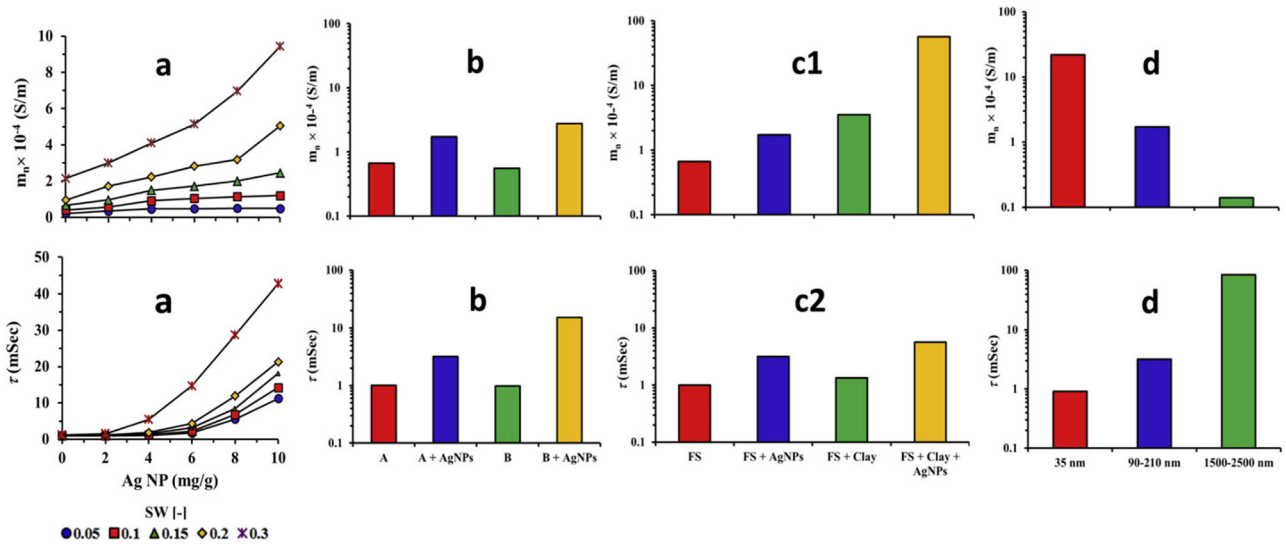

Fig. 7.

(1) Normalized chargeability (m_n) and (2) relaxation time (τ) resulting from the Cole-Cole model of the data of (a) the effect of AgNPs concentrations at different water saturation, (b) the effect of fluid chemistry, (c) the effect of lithology and (d) the effect of different grain size diameter of AgNPs. FS = fine sand. A, B = fluid types.

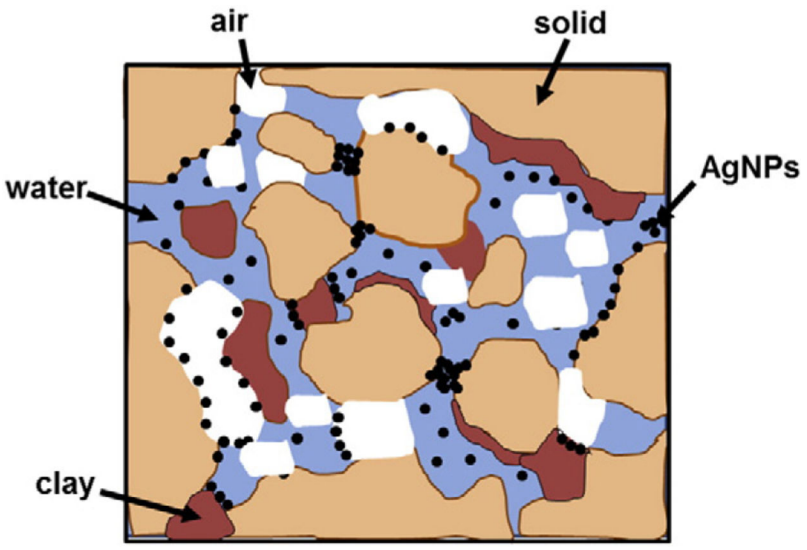

Fig. 8.

A summary of the various mechanisms affecting deposition and retention of environmental nanomaterials in partially saturated soil is depicted in this conceptual diagram, which includes processes governing environmental nanomaterials distribution and interactions within the soil environment. The major phases of the soil environment (soil solution, air and solid phases), and some of the major processes reported to affect environmental nanomaterials deposition and interaction in the soil system are also shown. (Adapted from Dror et al., 2015.)

Table 1

Experiment treatments, levels, and experimental numbers.

Experiment Number	Experimental treatments				
	Percent saturation (% AGW)	**AGW EC (S/m) ±0.003 S/m**	**AgNP concentration (mg/g)**	**Lithology**	**AgNP size (nm)**
I	5, 10, 15, 20, 30	Type A	0, 2, 4, 6, 10	Fine sand	90–120
II	15	Type A, Type B	0, 6	Fine sand	90–120
III	15	Type A	6	Fine sand, fine sand +6 mg/g kaolinite	90–120
IV	15	Type A	6	Fine sand	35, 90–210, 1500–2500

AGW = artificial ground water.

EC = electrical conductivity in S/m; Type A = 0.0275 ± 0.003, Type B = 0.1000 ± 0.003.

Table 2

Summary of power law fitted equations and correlation coefficients (R^2) for quadrature (σ'') and in-phase (σ') conductivity components at 10 Hz as a function of different silver nanoparticles concentrations (0, 2, 4, 6, 8, and 10 mg/g) for different water saturation (0.05, 0.10, 0.15, 0.20, and 0.30) in fine sand.

SW [−]	σ'' fitted equations	R^2	σ' fitted equations	R^2
0.05	$\sigma'' \times 10^{-6} = 0.541\ AgNP^{0.353}$ (mg/g)	0.97	$\sigma' \times 10^{-3} = 0.794\ AgNP^{0.256}$ (mg/g)	0.94
0.10	$\sigma'' \times 10^{-6} = 0.618\ AgNP^{0.798}$ (mg/g)	0.95	$\sigma' \times 10^{-3} = 0.742\ AgNP^{0.128}$ (mg/g)	0.36
0.15	$\sigma'' \times 10^{-6} = 0.776\ AgNP^{0.867}$ (mg/g)	0.95	$\sigma' \times 10^{-3} = 0.980\ AgNP^{0.084}$ (mg/g)	0.53
0.20	$\sigma'' \times 10^{-6} = 1.077\ AgNP^{0.920}$ (mg/g)	0.88	$\sigma' \times 10^{-3} = 1.298\ AgNP^{0.056}$ (mg/g)	0.21
0.30	$\sigma'' \times 10^{-6} = 1.216\ AgNP^{1.349}$ (mg/g)	0.93	$\sigma' \times 10^{-3} = 1.792\ AgNP^{0.116}$ (mg/g)	0.55